ABSTRACT

SEARCH FOR CHARGED HIGGS BOSONS IN THE $\tau + \ell$ FINAL STATE WITH 36.1 fb^{-1} OF pp COLLISION DATA AT $\sqrt{s} = 13$ TeV WITH THE ATLAS EXPERIMENT

Elliot Wesley Parrish, Ph.D.
Department of Physics
Northern Illinois University, 2022
Dhiman Chakraborty and Jahred Adelman, Director

This dissertation uses 139 fb^{-1} of pp collision data collected at a center of mass energy of $\sqrt{s} = 13$ TeV by the ATLAS detector to search for charged Higgs bosons decaying to a tau lepton and a neutrino ($H^{\pm} \to \tau^{\pm}\nu_{\tau}$) in association with a leptonically decaying top quark. No significant excess was found, therefore limits are set at the 95% confidence level on the charged Higgs production cross section times the branching fraction into the $\tau^{\pm}\nu_{\tau}$ ranging from XX pb to XX fb. These limits are interpreted in the hMSSM benchmark scenario as an exclusion at 95% confidence on $\tan\beta$ as a function of $m_{H^{\pm}}$. In this scenario, for $\tan\beta = 60$, the $H^{\pm}$ mass range up to XXX GeV is excluded, with all values of $\tan\beta$ excluded for $m_{H^{\pm}} \leq XXX$ GeV.

NORTHERN ILLINOIS UNIVERSITY
DE KALB, ILLINOIS

DECEMBER 2022

SEARCH FOR CHARGED HIGGS BOSONS IN THE $\tau + \ell$ FINAL STATE WITH 36.1 fb^{-1} OF pp COLLISION DATA AT $\sqrt{s} = 13$ TeV WITH THE ATLAS EXPERIMENT

BY

ELLIOT WESLEY PARRISH

A DISSERTATION SUBMITTED TO THE GRADUATE SCHOOL

IN PARTIAL FULFILLMENT OF THE REQUIREMENTS

FOR THE DEGREE

DOCTOR OF PHILOSOPHY

DEPARTMENT OF PHYSICS

Dissertation Director:
Dhiman Chakraborty and Jahred Adelman

ACKNOWLEDGEMENTS

DEDICATION

To Dr. Dhiman Chakraborty. Thank you for everything.

TABLE OF CONTENTS

Chapter Page

LIST OF TABLES

Table Page

LIST OF FIGURES

CHAPTER 1

INTRODUCTION

CHAPTER 2

THEORY

In this chapter, the theoretical motivation of a search for $H^{\pm} \to \tau^{\pm}\nu_{\tau}$ is described. Firstly, a review of the Standard Model of particle physics (SM) is laid out, then a brief overview of Supersymmetry focusing on the Minimal Supersymmetric Standard Model (MSSM). Finally, the Type II 2-Higgs Doublet Model's (2HDM) relation to the $H^{\pm}$ production cross section and subsequent branching ratio into SM particles is described as motivation for the choice of studying $H^{\pm} \to \tau^{\pm}\nu_{\tau}$.

2.1 The Standard Model

The Standard Model of particle physics is a quantum field theory that describes all known matter and forces. The Standard Model is built upon a gauge group of type $SU(3)_C \times SU(2)_L \times U(1)_Y$. The $SU(3)_C$ term dictates the strong interaction while the $SU(2)_L \times U(1)_Y$ term describes the electroweak interaction. These interactions occur between fundamental particles called fermions that comprise the known matter of the universe. The interactions, or forces, are mediated by fundamental particles called bosons.

2.1.1 Particles

The particles that make up the Standard Model are separated into two groups according to their intrinsic angular momentum charge, or spin. Fermions are those that carry half-integer spin, and thus obey Fermi-Dirac statistics, while Bosons carry full integer spin values and obey Bose-Einstein statistics.

2.1.1.1 Fermions

The matter we encounter in everyday life is comprised of fermions. Fermions are subdivided into two groups, quarks and leptons. The quarks participate in the strong interaction via their color charge. Quarks cannot exist as a singular particle and thus combine into hadrons in a process called hadronization; the bound states they form are colorless. The proton and neutron are examples of hadrons. Leptons carry no color charge and therefore do not participate in strong force interactions. The fermions in the SM all participate in the electroweak interaction. However, the electromagnetic interaction is limited to those fermions that carry an electromagnetic charge. Section 2.1.2.2 describes the electroweak interaction in detail.

Fermions can then be further divided into three generations, each lepton has an electrically neutral weak force partner in the form of a neutrino. Table 2.1 lists all the SM fermions and their properties.

2.1.1.2 Bosons

Bosons are colloquially referred to as force-carriers in that the fundamental forces act via exchanging gauge bosons. This means that each force has an associated boson which is described by a field theory. The ElectroWeak quantum field theory (QFT) is more complicated, and is described in detail in section 2.1.2.2. Table 2.2 lists the SM bosons [1], their associated field theory and properties.

[1] excluding the Higgs

Table 2.1: Standard Model fermions and their properties [1]

	1^{st} Generation	2^{nd} Generation	3^{rd} Generation	Spin	EM Charge	Color	Mass
Quarks	Up (u)	Charm (c)	Top (t)	$\frac{1}{2}$	$+\frac{2}{3}$	✓	$m_u = 2.16^{+0.49}_{-0.26}$ MeV $m_c = 1.27 \pm 0.02$ GeV $m_t = 172.76 \pm 0.30$ GeV
	Down (d)	Strange (s)	Bottom (b)	$\frac{1}{2}$	$-\frac{1}{3}$	✓	$m_d = 4.67^{+0.48}_{-0.17}$ MeV $m_s = 93^{11}_{-5}$ MeV $m_b = 4.18^{0.03}_{-0.02}$ GeV
Leptons	Electron (e^-)	Muon (μ^-)	Tau (τ^-)	$\frac{1}{2}$	-1	X	$m_{e^-} = 0.51$ MeV $m_{\mu^-} = 105.65$ MeV $m_{\tau^-} = 1776.86 \pm 0.12$ MeV
	Electron Neutrino (ν_e)	Muon Neutrino (ν_μ)	Tau Neutrino (ν_τ)	$\frac{1}{2}$	0	X	$m_{\nu_e} < 1.1$ eV $m_{\nu_\mu} < 0.19$ MeV $m_{\nu_\tau} < 18.2$ MeV

Table 2.2: Standard Model bosons and their properties [1]

Field Theory	Boson	Spin	EM Charge	Color	Mass
Quantum Chromodynamics (QCD)	Gluon (g)	1	0	✓	0
Quantum Electrodynamics (QED)	Photon (γ)	1	0	X	$< 1\,\mathrm{x}\,10^{-18}$ eV
ElectroWeak Theory	$W^\pm$	1	±1	X	80.379 ± 0.012 GeV
	Z^0	1	0	X	91.1876 ± 0.0021 GeV

2.1.2 Interactions

At its core, the SM relies upon symmetries. From these symmetries, conservation laws follow. It is these laws of conservation, and the breaking of tthe associated symmetry, that dictate the allowed interactions of matter. The first, being a symmetry under charge conjugation, mirror reflection, and time reversal is known as CPT symmetry. The symmetry between charge conjugation and mirror reflection (CP) can be broken in certain circumstances, but holds in strong and electromagnetic interactions. This breaking of CP symmetry occurs in the weak interaction and implies a non-symmetry between matter and antimatter. Since this symmetry holds for strong and electromagnetic interactions, baryon number ($B = \frac{1}{3}(n_q - n_{\bar{q}})$) and lepton number are conserved in SM interactions. Lepton generation number [2], electric charge, color charge, 4-momentum ($p = (E, \vec{p})$), and angular momentum are all conserved in the SM.

2.1.2.1 Quantum Electrodynamics

The electromagnetic force is governed by the QFT known as Quantum Electrodynamics (QED). This force is mediated by the photon, γ, a massless boson with EM charge 0. The EM force only affects, in other words, the photon only interacts with, charged particles; including all quarks and the e, μ, and τ leptons. Antiparticles are those that carry the opposite EM charge from their normal counterparts and differ in no other way. Antiparticles are denoted by a bar above the particle symbol ($e, \bar{e}$).

[2] Ignoring neutrino oscillations

2.1.2.2 ElectroWeak Interaction

The weak force is most often seen in nuclear decays and is mediated by the $W^{\pm}$ and Z^0 bosons. Due to the relatively large mass of these bosons, the weak force has a very limited range. The $W^{\pm}$ affects the third component of isospin (T_3), thus only coupling to so called left-handed fermions. This "handedness", or chirality, is a property similar to color charge, in that an individual particle can have a number of different values. Table 2.3 contains the allowed values for isospin (T) and hypercharge (Y_W).

Table 2.3: Standard Model fermions and their ElectroWeak properties [1]

	1^{st} Generation	2^{nd} Generation	3^{rd} Generation	EM Charge	Y_W		T		T_3	
					LH	RH	LH	RH	LH	RH
Quarks	Up (u)	Charm (c)	Top (t)	$+\frac{2}{3}$	$+\frac{1}{3}$	$+\frac{4}{3}$	$\frac{1}{2}$	0	$\pm\frac{1}{2}$	0
	Down (d)	Strange (s)	Bottom (b)	$-\frac{1}{3}$	$+\frac{1}{3}$	$-\frac{2}{3}$	$\frac{1}{2}$	0	$\pm\frac{1}{2}$	0
Leptons	Electron (e^-)	Muon (μ^-)	Tau (τ^-)	-1	-1	0	$\frac{1}{2}$	0	$\pm\frac{1}{2}$	0
	Electron Neutrino (ν_e)	Muon Neutrino (ν_μ)	Tau Neutrino (ν_τ)	0	-1	-2	$\frac{1}{2}$	0	$\pm\frac{1}{2}$	0

The $W^{\pm}$ bosons have a T_3 component of isospin and act as raising or lowering operators on the T_3 component of left handed fermions. The Z does not have a T_3 component, and thus does not act on isospin of fermions. However, the Z boson instead transfers momentum, energy, and spin on all fermions irregardless of their chirality. At energies $>$ 100 GeV the electromagnetic and weak forces combine into the electroweak force. In fact, isospin and hypercharge combine to give electromagnetic charge. $Q_{EM} = T_3 + \frac{1}{2}Y_W$

2.1.2.3 Quantum Chromodynamics

Quantum chromodynamics (QCD) is the QFT that describes the strong force that holds together atomic nuclei and other objects called hadrons. The strong force interacts via the color charge [3] which can have values of either red, green, or blue. Particles that have a color charge cannot exist on their own, they must form colorless bound states called hadrons. Since the strong force grows with distance, if a quark is ejected out from a hadron, the stored energy is such that new particles with color charge will be spontaneously created from the vacuum, binding with the free quark in a process called hadronization. In a particle detector, the hadronization process cascades and creates showers of hadrons that are reconstructed as so called jets.

2.1.3 The Higgs Mechanism

The Higgs field is the mass generator of the SM and was first theorized by Peter Higgs [2], François Englert, and Robert Brout [3] in 1964. The SM itself has four massless Goldstone bosons that do not correspond to the observed bosons. Instead, the Higgs mechanism couples to them via a complex scalar doublet.

$$\phi = \begin{pmatrix} \phi^+ \\ \phi^0 \end{pmatrix} \tag{2.1}$$

The scalar potential that gives rise to this phenomena can be written as

$$V(\phi) = \mu^2|\phi^\dagger\phi| + \lambda(|\phi^\dagger\phi|)^2 \tag{2.2}$$

[3]This color does is not the visual color we are used to. Merely a convenient analogous naming scheme.

When $\mu^2 > 0$ and $\lambda > 0$ the minimum of the potential $V(\phi)$ is 0. However, when $\mu^2 < 0$,

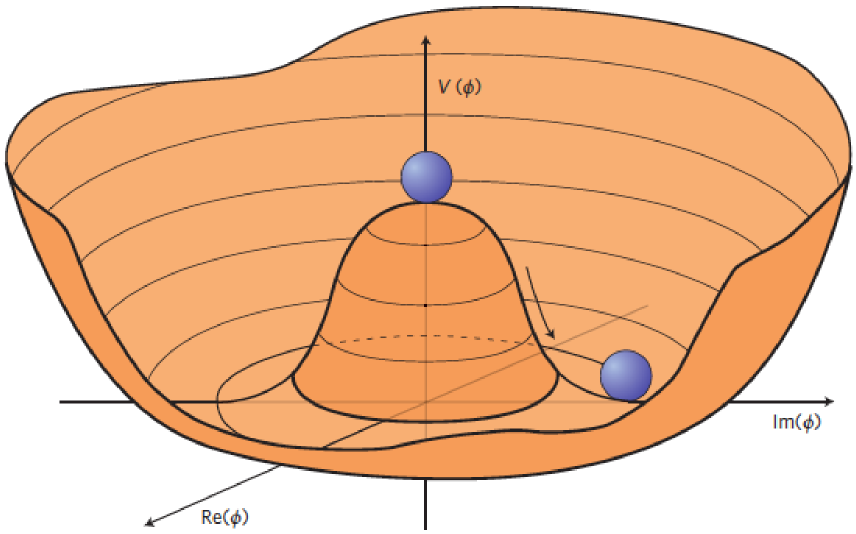

Figure 2.1: The Higgs potential defined in 2.2 with $\mu^2 < 0$ [4]

the scalar potential $V(\phi)$ takes the shape shown in figure 2.1 It follows that the vacuum expectation value (VEV) of ϕ is then

$$\langle\phi\rangle = \sqrt{\frac{-\mu^2}{2\lambda}} = \frac{\nu}{\sqrt{2}} \tag{2.3}$$

From here, convention states that we choose an arbitrary direction of the fluctuation as

$$\phi^0 = \frac{1}{\sqrt{2}}\binom{0}{\nu} \tag{2.4}$$

By choosing these values, $SU(2)$ and $U(1)_Y$ symmetries are broken, the Goldstone bosons are "eaten" and we are left with the remaining degree of freedom being the real scalar field $h(x)$

$$\phi(x) = \phi^0 + h(x) \tag{2.5}$$

Substituting in our definition of ϕ^0, we get

$$\phi = \frac{1}{\sqrt{2}}\begin{pmatrix} 0 \\ \nu + h(x) \end{pmatrix} \tag{2.6}$$

and couples to the gauge bosons via

$$(\frac{1}{2}g\vec{\sigma}\cdot\vec{W} + \frac{1}{2}g'B)\phi^0 \tag{2.7}$$

, where $\vec{\sigma}$ are the Pauli matrices, $\vec{W}$ are $W_{1,2,3}$, g is the weak coupling constant, and $g\prime$ is the hypercharge coupling constant. From this coupling, we get the four eigenstates that correspond to the observed bosons

$$\begin{aligned} W^{\pm} &= \frac{1}{\sqrt{2}}(W^1_\mu \mp iW^2_\mu) \\ Z^\mu &= \frac{-g\prime B_\mu + gW^3_\mu}{\sqrt{g^2 + g\prime^2}} \\ A^\mu &= \frac{gB_\mu + g\prime W^3_\mu}{\sqrt{g^2 + g\prime^2}} \end{aligned} \tag{2.8}$$

These eigenstates have corresponding mass values of

$$\begin{aligned} M_W^2 &= \frac{1}{4}g^2\nu^2 \\ M_Z^2 &= \frac{1}{4}(g^2 + g\prime^2)\nu \\ M_A^2 &= 0 \end{aligned} \tag{2.9}$$

The eigenstate labeled here as A is the photon. The Higgs boson was discovered in 2012 by the ATLAS and CMS collaborations at CERN with a mass of 125 GeV [5]. The scalar boson that was found appears to be the SM Higgs Boson.

2.2 Supersymmetry

While the Standard Model is describes a wide range of physics to a high degree of accuracy, it is not without issues. To name a few, gravity, dark matter, and the observed matter-antimatter asymmetry of the universe are not defined by the SM. In addition, the SM defines the mass of neutrinos to be 0. However, because neutrino mixing is observed, where $\nu_e \rightarrow \nu_\mu$ is seen, neutrinos must have mass.

One promising model that offers solutions to many of these issues is Supersymmetry (SUSY). As discussed previously, the SM is built upon symmetries, and the breaking of these symmetries gives us electroweak unification. SUSY proposes another symmetry, this time between fermions and bosons.

$$\begin{aligned} Q|Fermion\rangle &= |Boson\rangle, \\ Q|Boson\rangle &= |Fermion\rangle \end{aligned} \tag{2.10}$$

Equation 2.10 shows how the SUSY operator Q acts on particles. SUSY naturally offers solutions to the “hierarchy problem” with the SM.

The hierarchy problem arises from the difference in electroweak ($M_W \sim 100$ GeV) and Planck ($M_P \sim 2.4 \,\text{x}\, 10^{18}$ GeV) mass scales. For the Higgs mass to be on the scale of $M_H \sim 125$ GeV incredibly large and small mass terms must cancel perfectly, leading to a feeling of “unnaturalness”. SUSY brings many new particles into the picture, theorized to occupy the intermediate mass range leading to a more natural theory.

2.2.1 MSMM Particles

SUSY is a large group of theories, including many additional superpartner particles. The Minimal Supersymmetric Standard Model (MSSM) is the smallest extension of the SM that introduces SUSY. In the MSSM, each SM particle is part of a supermultiplet with it's superpartner where both particles have the same quantum numbers, except spin. If this supersymmetry is unbroken, then the superpartner and the SM particle would have the same mass as well. However, SUSY has not been observed, so the supersymmetry must be broken putting the mass scale on the TeV scale.

Table 2.4: SM particles and their MSSM partners [1]

Name	SM	MSSM
Spin-$\frac{1}{2}$ quarks and spin-0 squarks		
(s)up	u	$\tilde{u}$
(s)down	d	$\tilde{d}$
(s)charm	c	$\tilde{c}$
(s)strange	s	$\tilde{s}$
(s)top	t	$\tilde{t}$
(s)bottom	b	$\tilde{b}$
Spin-$\frac{1}{2}$ leptons and spin-0 sleptons		
(s)electron	e	$\tilde{e}$
(s)electron (s)neutrino	ν_e	$\widetilde{\nu_e}$
(s)muon	μ	$\tilde{\mu}$
(s)muon (s)neutrino	ν_μ	$\widetilde{\nu_\mu}$
(s)tau	τ	$\tilde{\tau}$
(s)tau (s)neutrino	ν_τ	$\widetilde{\nu_\tau}$
Spin-0 Higgs and spin-$\frac{1}{2}$ Higgsinos		
Higgs(ino)	H	$\tilde{H}$
gluon (gluino)	g	$\tilde{g}$
W (Wino)	$W^{\pm}$, W^0	$\widetilde{W^{\pm}}, \widetilde{W^0}$
B (Bino)	B^0	$\widetilde{B^0}$

Table 2.4 lists the MSSM supermultiplets and the associated naming conventions.

2.2.2 2 Higgs Doublet Model

Having only one Higgs chiral supermultiplet with hypercharge $Y_W = \pm\frac{1}{2}$ leads to a gauge anomaly. This can be resolved by introducing two Higgs doublets with hypercharge $Y_W = \frac{1}{2}$ and $Y_W = -\frac{1}{2}$. Such is the case with the MSSM which requires two complex doublet scalar fields where one couples to the up-type quarks and the other couples to down-type quarks and charged leptons. At this point, the MSSM has 8 degrees of freedom. Following the same type of symmetry breaking described in subsection 2.1.3 Three of these degrees of freedom give the observed $W^{\pm}$ and Z^0 bosons. This leaves us with the extended Higgs sector shown

Table 2.5: 2HDM extended Higgs sector [6]

light neutral scalar	h^0
heavy neutral scalar	H^0
neutral pseudoscalar	A^0
two charged scalars	$H^{\pm}$

in table 2.5, where the h^0 is the SM-like Higgs that was discovered by ATLAS and CMS in 2012. When referring to the charged Higgs bosons, we often refer to them using one symbol $H^{\pm}$. In the 2HDM we have two free parameters[4], the masses of the $H^{\pm}$ and the ratio of their vacuum expectation values which is defined as $\tan\beta$.

2.3 Charged Higgs Bosons

Since the $H^{\pm}$ couplings are proportional to the fermion masses, the main production modes at the LHC are through $t\bar{t}$and Wt diagrams where the W is replaced by a $H^{\pm}$. The production diagrams considered in this dissertation can be seen in figure 2.3. The cross section at various $\tan\beta$ values can be seen as a function of $m_{H^\pm}$ in figure 2.4. As $\tan\beta$ goes to smaller values the $H^\pm$ cross section become smaller and at very small values the top Yukawa couplings become non-perturbative, meaning they are highly unlikely to occur. In this dissertation the decay channel considered is $H^\pm \rightarrow \tau^\pm\nu_\tau$. As can be seen in figure 2.5, the $H^\pm \rightarrow \tau^\pm\nu_\tau$ decay channel is especially relevant at low $m_{H^\pm}$ and high $\tan\beta$. The search described in this dissertation consists of two sub-channels, τ+jets and $\tau + \ell$, where the associated top decays either hadronically or leptonically respectively.

2.3.1 Previous Result

To add context to this dissertation, it is important to reference the results of the previous iteration of the search discussed in this dissertation. The ATLAS collaboration published a paper in 2018 covering the data taking years of 2015 and 2016 [8], whereas this dissertation covers the full Run-2 (2015-2018) dataset. Figure 2.6 shows the limits on the cross section and figure 2.7 shows the limits on $\tan\beta$ as a function of $m_{H^\pm}$.

The previous iteration of this analysis used boosted decision trees (BDT) binned in $m_{H^\pm}$, giving them five separate classifiers to cover the mass range of $90 - 2000$ GeV. The mass bins can be seen as the blue dotted lines in Figure 2.6c. It is important to note the inclusion of the mass range $90 - 200$ GeV, as [8] was the first search to include this mass region below the top quark mass of 175 GeV.

[4] Only regarding the charged Higgs bosons

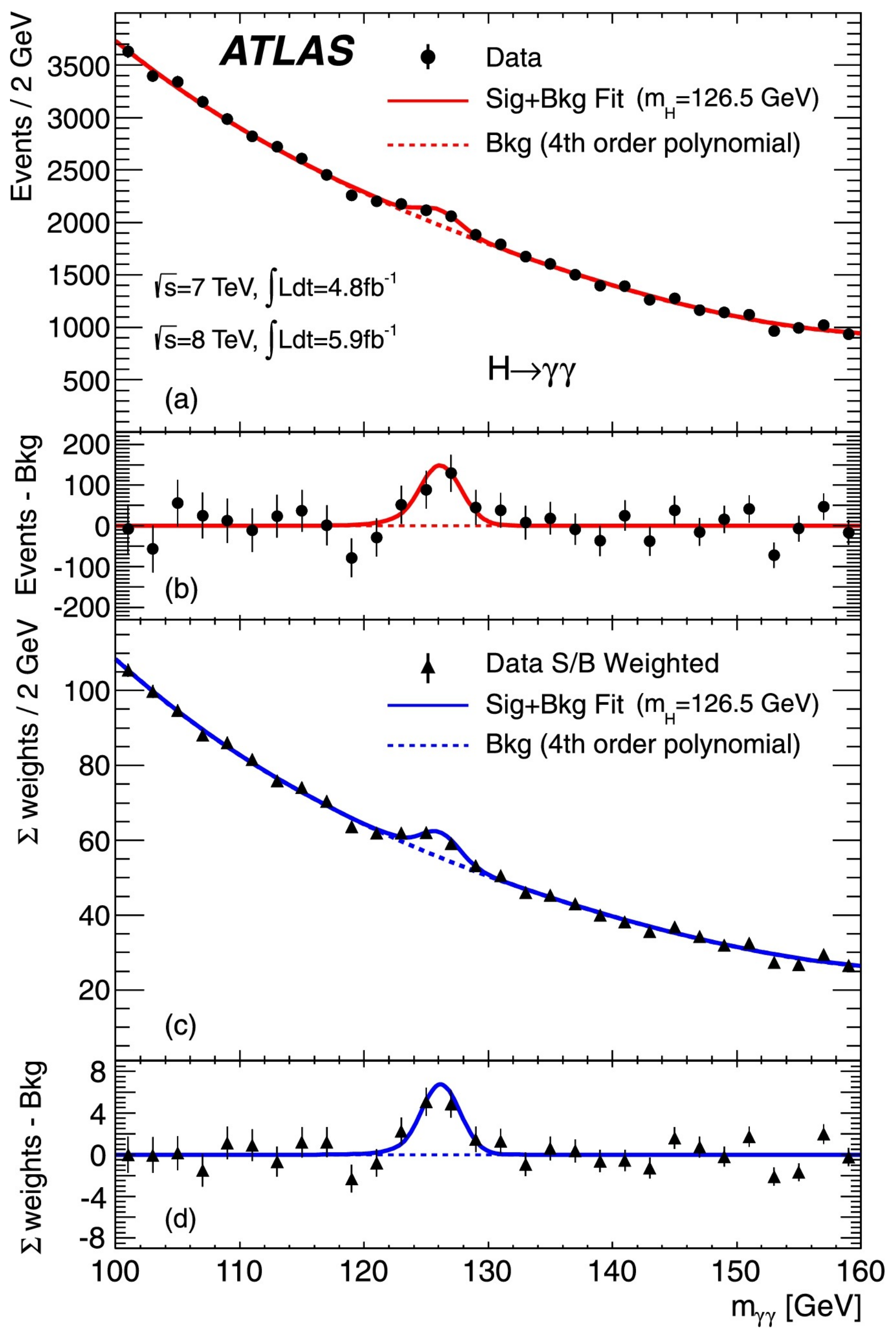

Figure 2.2: The distributions of the invariant mass of diphoton candidates after all selections for the combined 7 TeV and 8 TeV data sample. The inclusive sample is shown in (a) and a weighted version of the same sample in (c); the weights are explained in the text. The result of a fit to the data of the sum of a signal component fixed to $m_H = 126.5$ GeV and a background component described by a fourth-order Bernstein polynomial is superimposed. The residuals of the data and weighted data with respect to the respective fitted background component are displayed in (b) and (d).

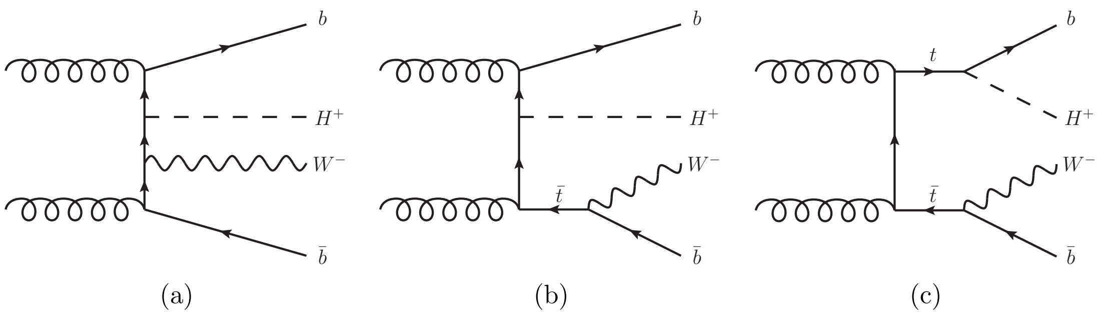

Figure 2.3: Examples of leading-order Feynman diagrams contributing to the production of charged Higgs bosons in pp collisions: (a) non-resonant top-quark production, (b) single-resonant top-quark production that dominates at large $H^{\pm}$ masses, (c) double-resonant top-quark production that dominates at low $H^{\pm}$ masses. The interference between these three main diagrams becomes most relevant in the intermediate-mass region.

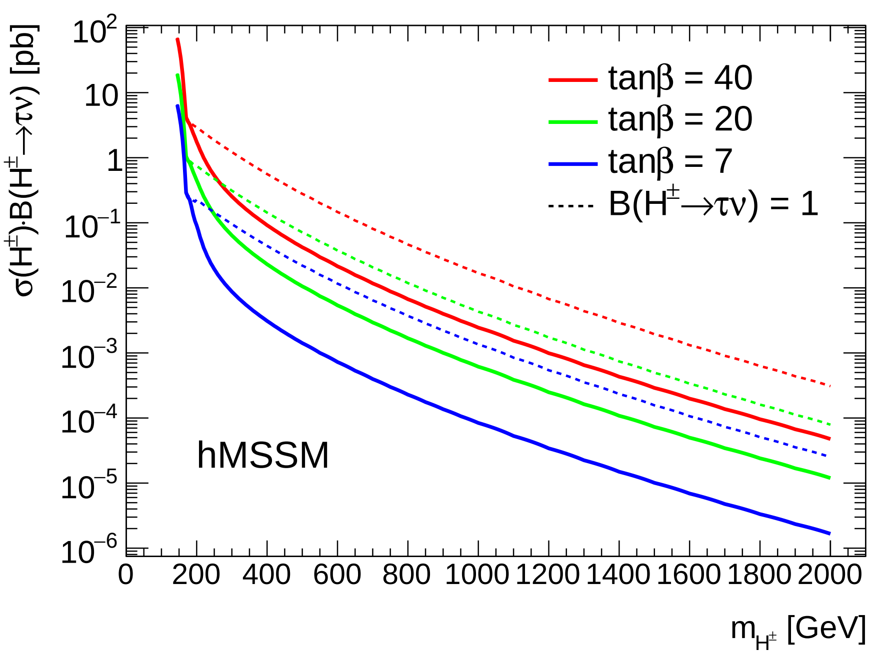

Figure 2.4: Cross section of $H^{\pm}$ at various $\tan\beta$ values.

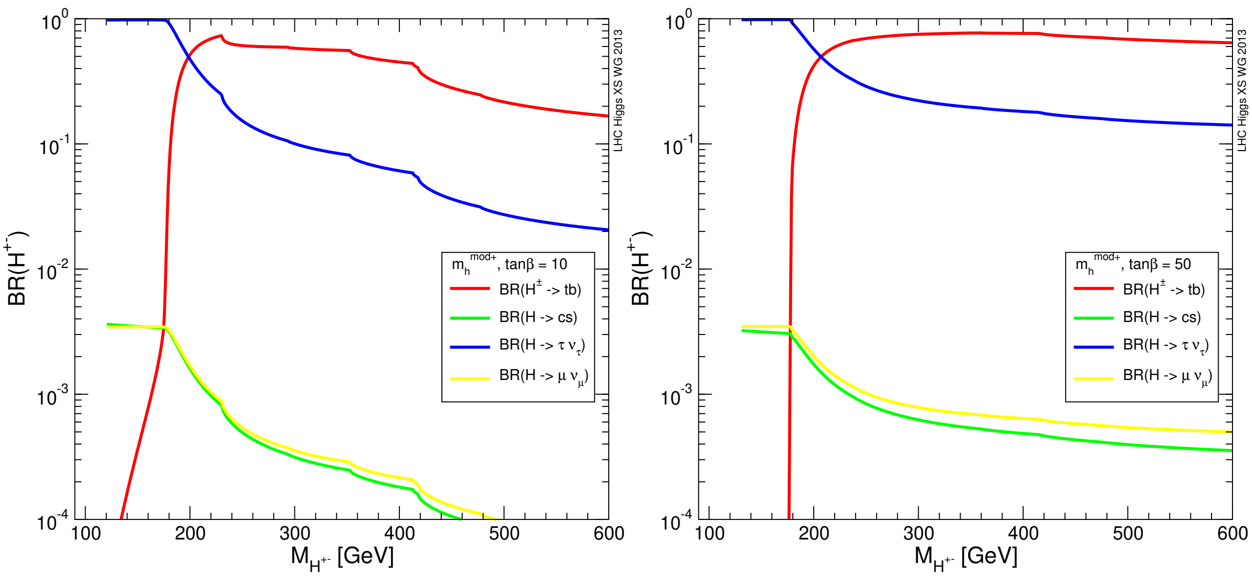

(a) (b)

Figure 2.5: Branching ratios of $H^{\pm}$ for (a) $\tan\beta = 10$ and (b) $\tan\beta = 50$ [7]

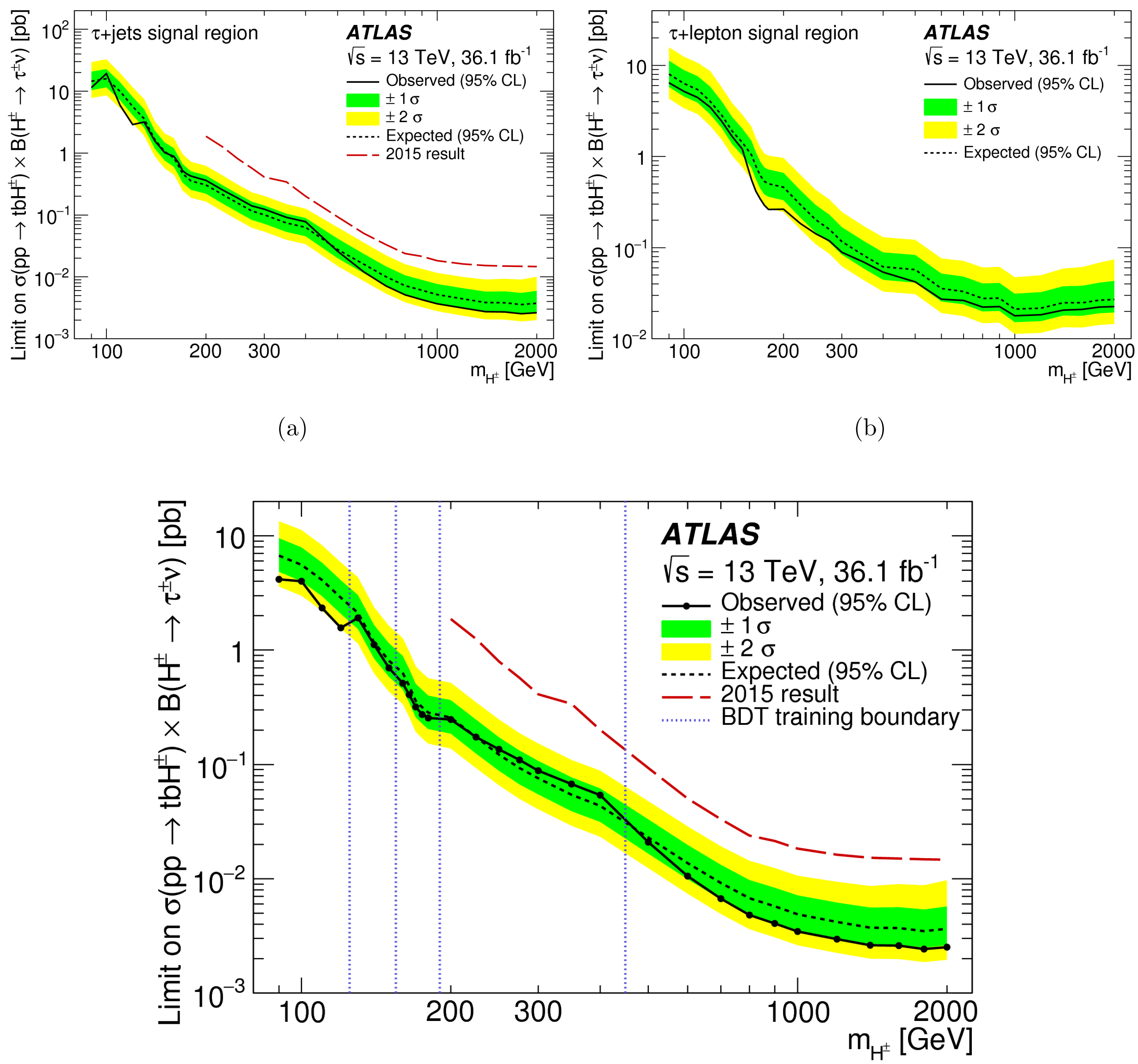

(a) (b) (c)

Figure 2.6: Limits on $\sigma(pp \to tbH^{\pm}xB(H^{\pm} \to \tau^{\pm}\nu))[pb]$. (a) is for the τ+jets subchannel (b) corresponds to the $\tau + \ell$ subchannel and (c) is the combination of the two subchannels. [8]

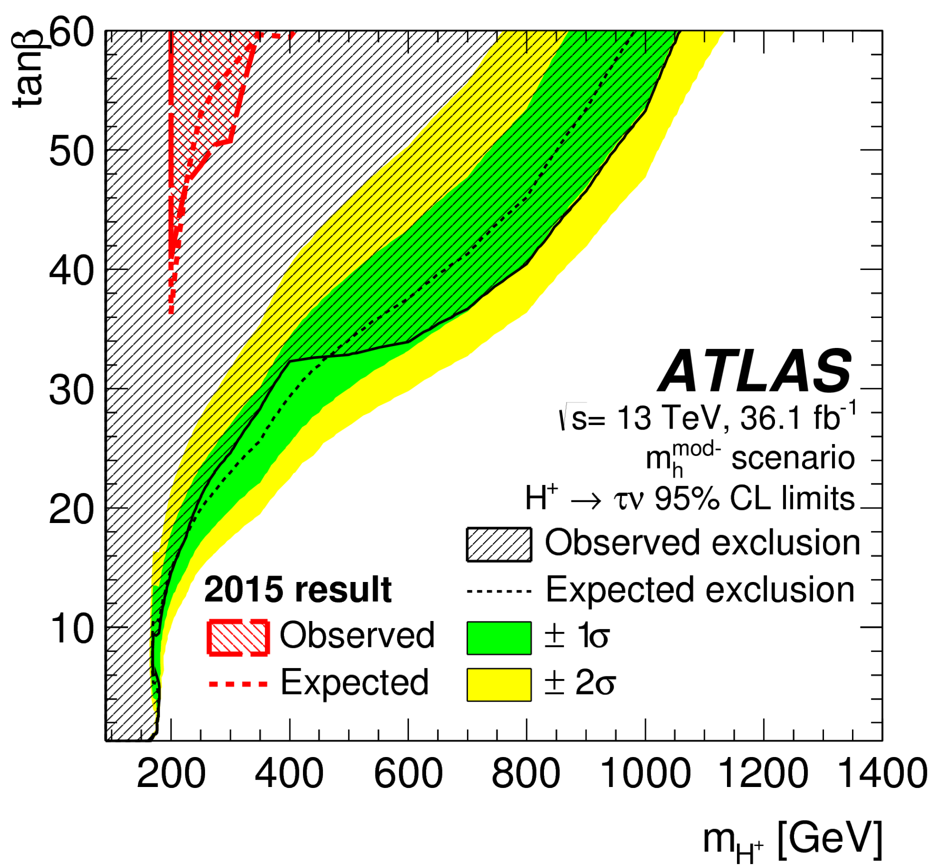

Figure 2.7: Limits on $\tan\beta$ as a function of $m_{H^{\pm}}$. [8]

CHAPTER 3
EXPERIMENTAL APPARATUS

3.1 Particle Accelerators

To study the Standard Model, the Higgs boson, and hints of new physics, particle accelerators are used. Particle accelerators can be categorized as either fixed target or colliders. As the naming suggest, in a fixed target accelerator the beam hits a target that then produces the desired particle collisions. Whereas a collider uses two opposite circulating beams that are then brought to collide inside a detector. A fixed target accelerator energy scales as $E_{CM} = \sqrt{E_{beam}}$ whereas a collider scales as $E_{CM} = 2\,E_{beam}$.

3.1.1 Hadron Colliders

There are two main types of particle colliders, those that use hadrons and those that use leptons. Lepton colliders are often referred to as precision machines, as the longitude momentum is known and backgrounds are well understood. The center of mass energy is well controlled in a lepton collider, meaning particles can be produced on resonance. On the other hand, due to the nature of hadrons not being fundamental particles a hadron collider produces a wide range of collisions. The constituents of a hadron participate in the collisions, meaning it is impossible to know the exact longitude momentum of the initial state. It is because of this exact reason that hadron colliders are referred to as discovery machines. The synchrotron radiation produced from a hadron collider is much lower than that of a lepton collider; meaning the beams are easier to control and can be pushed to higher energies without extra loses. The center of mass energy scales with $\frac{1}{m^4}$ in a hadron collider; again leading to an increased energy gain by simply using heavier particles.

3.1.2 The Large Hadron Collider

The Large Hadron Collider (LHC) is a 27 km circumference circular collider built outside of Geneva, Switzerland at CERN (Conseil Européen pour la Recherche Nucléaire). At center of mass energy 13.6 TeV, the LHC is the largest and highest energy particle accelerator ever built. There are four main collision points along the LHC: the ATLAS, CMS, ALICE, and LHCb experiments. ATLAS and CMS are general purpose particle detectors while ALICE and LHCb focus on heavy ion collisions. The numbers stated in the following sections are in reference to proton-proton collisions.

The LHC consists of 1104 NbTi superconducting dipole magnets, each being 15 m long, weighing 35 tonnes, cooled to 2 K, operating at 11,000 Amps, and produce a magnetic field of 8.3 T. A cross-section of a dipole magnet and the surrounding cryogenic system can be see in figure 3.1. The dipole magnets are used to bend the beam around the ring with another 128 used in the beam dump system to remove the beam safely from the LHC. A 2-in-1 configuration is used within the dipole magnets to create the required magnetic fields to bend two equally charged beams in opposite directions. A diagram of the magnetic fields in this configuration produced can be seen in 3.2. To focus the beam in the horizontal and vertical planes two quadrapole magnets are used; one magnet focuses in one plane while defocusing in the other. The end result is a horizontally and vertically focused beam. While in the LHC, the hadrons are accelerated using radiofrequency cavities. Table 3.1 lists some information on the LHC.

Table 3.1: LHC parameters [9]

Circumference	$26,659$ m
Dipole operating temperature	1.9 K
Dipole magnets	1232
Quadrapole magnets	392
Radiofrequency cavities	16 (8 per beam)
Beam energy	6.5 TeV (13 CoM TeV)
Protons per bunch	$1.2\text{x}10^{1}1$
Bunches per beam	2808
Revolutions per second	11245
Collisions per second	$1,000,000,000$

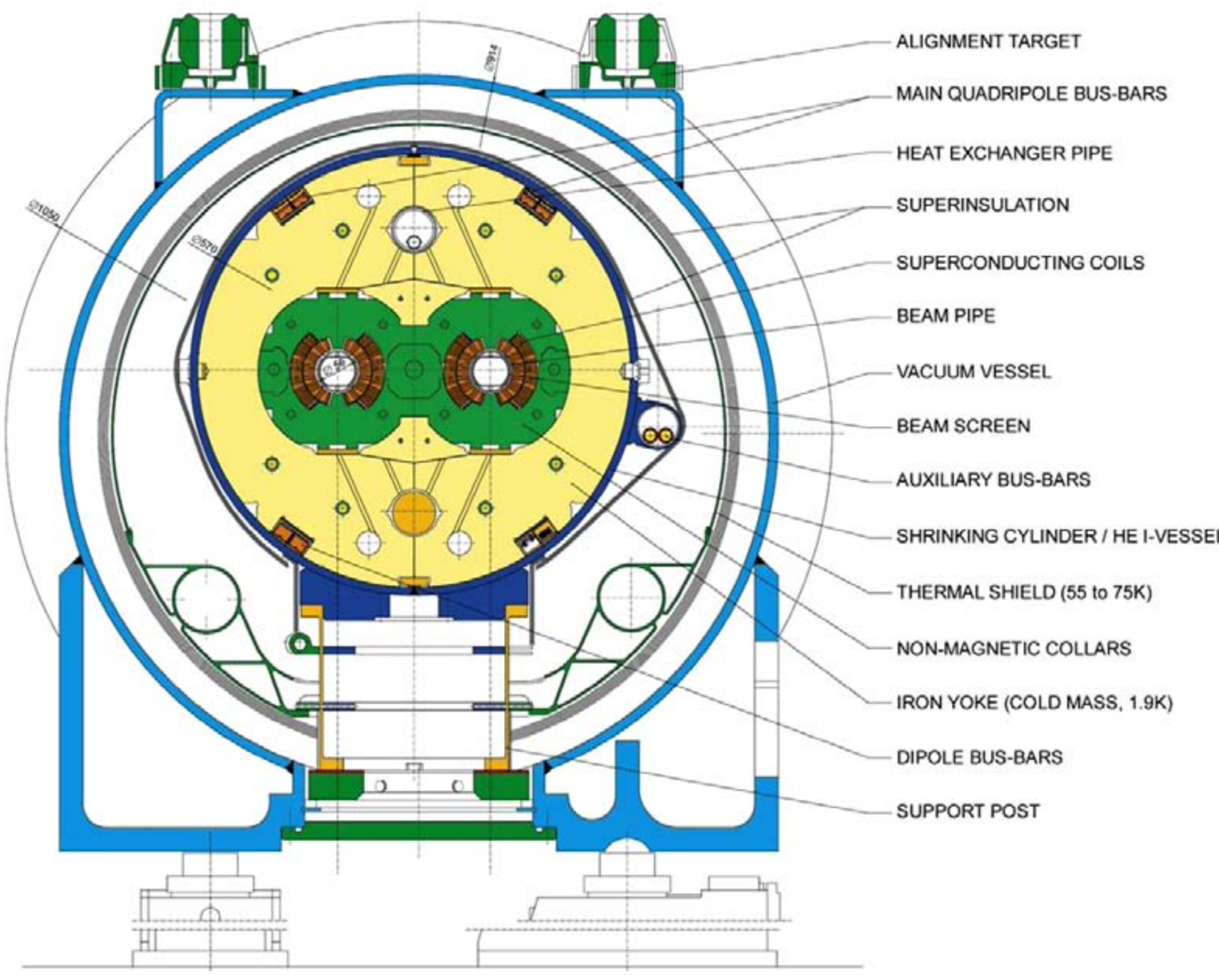

Figure 3.1: Cross-section of cryodipole (lengths in mm). [10]

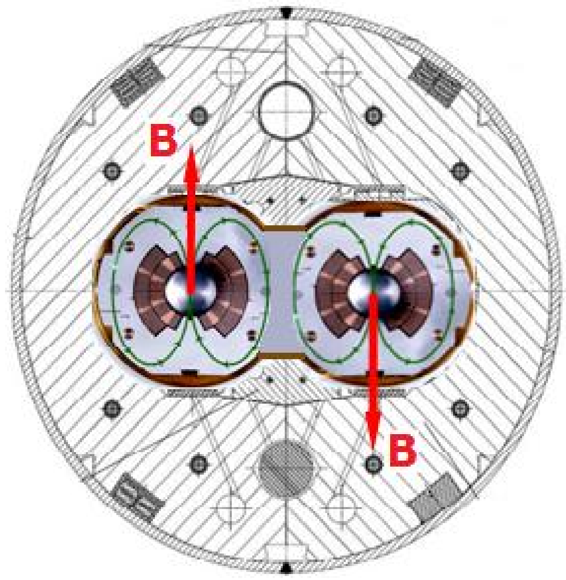

Figure 3.2: Field of the LHC dipole magnets. [11]

3.1.3 CERN Accelerator Complex

There are a series of accelerators used to get each beam up to its final energy of 6.5 TeV. The protons used in collisions are sourced from hydrogen atoms. The hydrogen is ionized, leaving the nucleus consisting of one proton, these protons are then accelerated in radiofrequency (RF) cavities. Figure 3.3 shows in detail the full accelerator complex at CERN. The protons used in the LHC start the accelerating process in the linear accelerator LINAC 2. They then are accelerated in the booster, PS, SPS, and are finally injected at the LHC where they are accelerated to the final 6.5 TeV beam energy. The final energies of protons from each accelerator can be seen in Table 3.2.

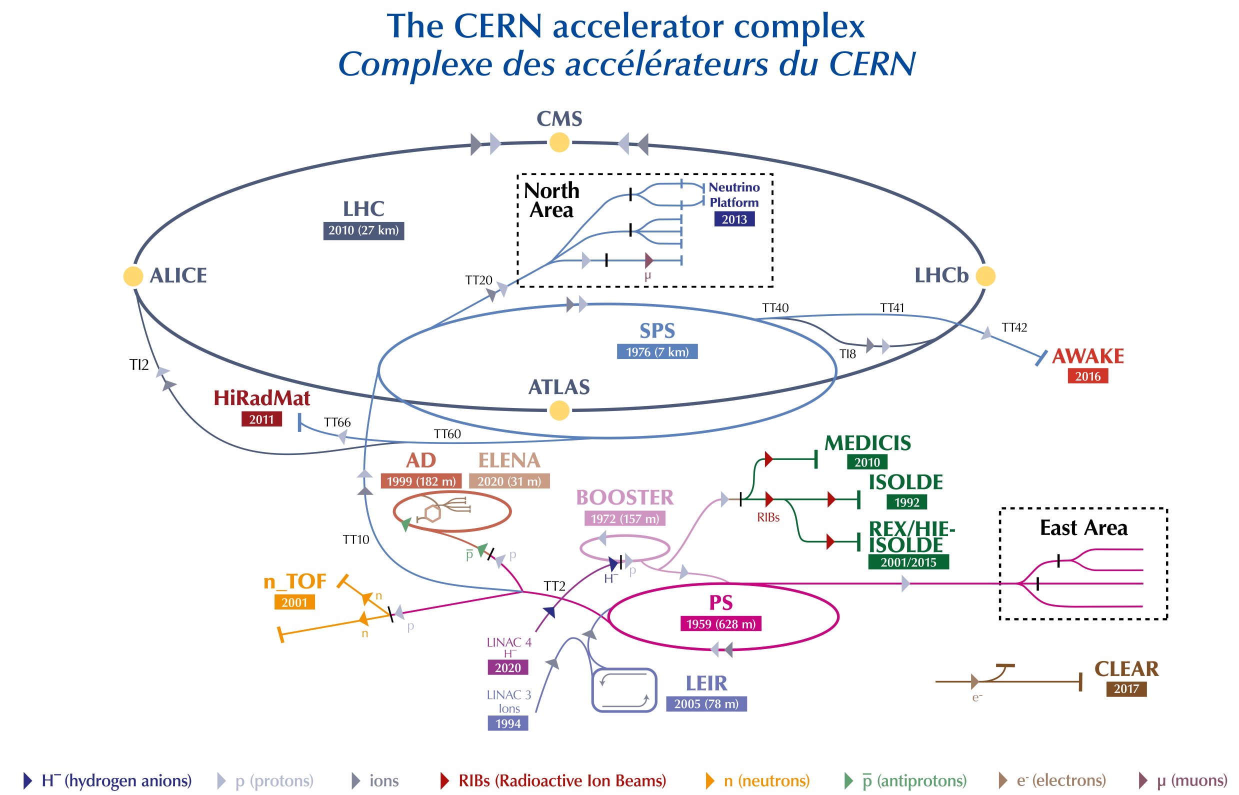

[redacted]

Figure 3.3: The CERN accelerator complex. [12]

Table 3.2: Accelerator final energies

Accelerator	Final Energy
LINAC 2	50 MeV
Booster	1.4 GeV
Proton Synchrotron (PS)	26 GeV
Super Proton Synchrotron (SPS)	450 GeV
Large Hadron Collider (LHC)	6.5 TeV

3.1.4 Luminosity

The amount of data collected from colliders is often referred to in terms of luminosity. Luminosity is measured in terms of inverse barns, where $1\,b = 10^{-28}\,m^2$. Instantaneous luminosity of one bunch crossing can be written as

$$\mathcal{L}_{bunch} = \frac{\mu f}{\sigma} \tag{3.1}$$

where σ is the cross section and can be thought of as the probability of a collision occurring, μ is the number of inelastic interactions per bunch crossing, and f is the revolution frequency of the LHC $f = 11246$ Hz. Therefore, the total instantaneous luminosity is

$$\mathcal{L} = N_b \frac{\langle\mu\rangle f}{\sigma} \tag{3.2}$$

where $\langle\mu\rangle$ is the average number of inelastic interactions per bunch crossing.

The integrated luminosity then corresponds to the total amount of data that was taken during a time period and can be seen for the LHC Run-2 in 3.4 The value of $\langle\mu\rangle$ changed throughout data taking and can be seen in Figure 3.5 and is referred to as pileup because the higher the $\langle\mu\rangle$ value, the more messy a collision becomes.

A common calculation using the total integrated luminosity is shown in Equation 3.3; where the number of times a particular process was produced is calculated.

$$N_x = \mathcal{L}\sigma_x \tag{3.3}$$

where again, σ is the cross section. In this case, the cross section corresponding to process x.

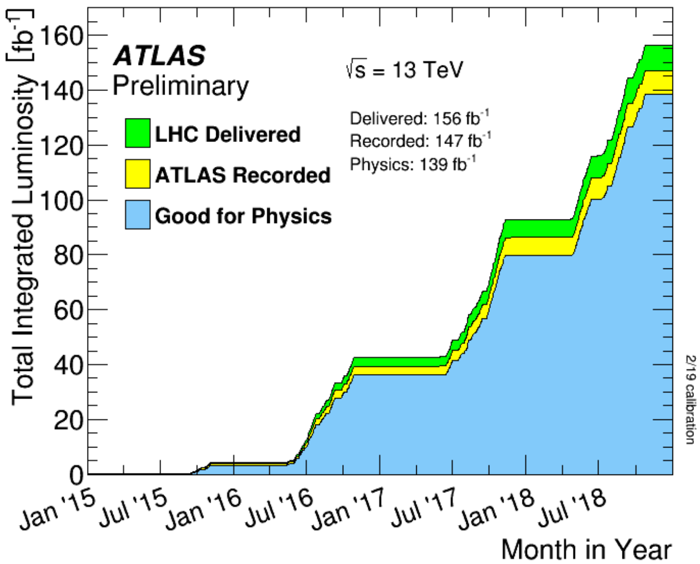

Figure 3.4: Cumulative luminosity versus time delivered to ATLAS (green), recorded by ATLAS (yellow), and certified to be good quality data (blue) during stable beams for pp collisions at 13 TeV center of mass energy in 2015-2018. The difference between the colored histograms reflects inefficiencies, especially those seen when restarting data taking.

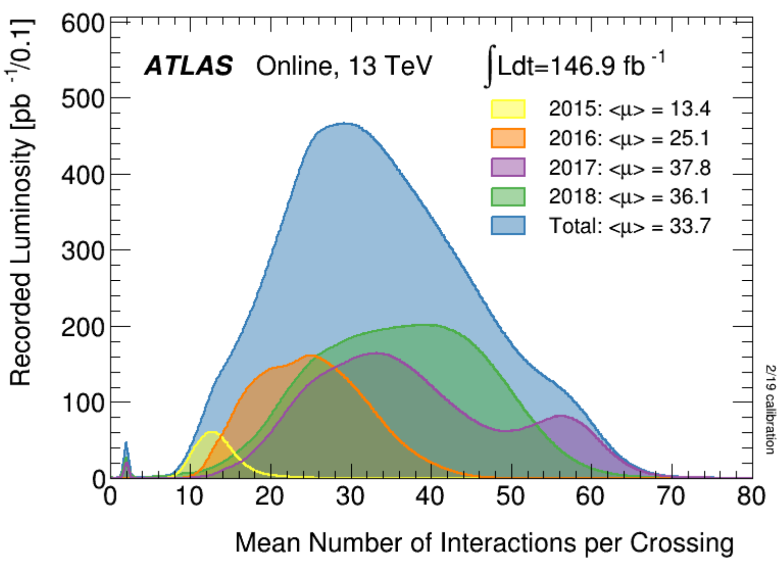

Figure 3.5: The luminosity-weighted distribution of the mean number of interactions per bunch crossing for the 2015-2018 pp collision dataset at 13 TeV center of mass energy.

3.2 The ATLAS Detector

3.2.1 Detector Coordinates

Since ATLAS is a cylinder, it is convenient to start with polar cylindrical coordinates. For ATLAS, the z-axis is inline with the beam line, the x-axis points towards the center of the LHC ring, and the y-axis points vertically. However, since particle collisions are relativistic by nature, a set of Lorentz invariant coordinates is much more useful. The radial coordinate r defines the radial distance from the interaction point (IP) at the center of ATLAS, ϕ is the azimuthal angle describing the angle from the x-axis in, and η, the pseudorapidity, is defined as

$$\eta \equiv -ln(tan(\frac{\theta}{2})) \tag{3.4}$$

where θ is the angle from the y-axis. It is in the differences in η between particles that provides the Lorentz invariance in this coordinate system of (r, ϕ, η). Due to the large collision energies of the LHC, the pseudorapidity is a close estimate to the true rapidity of the particles.

$$y \equiv \frac{1}{2}ln(\frac{E + p_Z}{E - p_Z}) \approx \eta \tag{3.5}$$

When speaking of differences in particle locations within ATLAS, ΔR is often used.

$$\Delta R \equiv \sqrt{(\Delta\eta)^2 + (\Delta\phi)^2} \tag{3.6}$$

3.2.2 Inner Detector

3.2.2.1 Pixel

3.2.2.2 Semiconductor Tracker

3.2.2.3 Transition Radiation Tracker

3.2.3 Calorimeters

3.2.3.1 Liquid Argon Electromagnetic Calorimeter

3.2.3.2 Tile Hadronic Calorimeter

3.2.4 Muon System

3.2.4.1 Monitored Drift Tubes

3.2.4.2 Cathode Strip Chambers

3.2.4.3 Resistive Plate Chambers

3.2.4.4 Thin Gap Chambers

3.2.5 Magnet Systems

CHAPTER 4

EVENT RECONSTRUCTION

4.1 Trigger

4.2 Inner Detector

4.3 Calorimeters

4.4 Muon

4.5 e γ

4.6 Jets

4.6.1 Flavor Tagging

4.6.2 τ

4.7 $E_{\mathbf{T}}^{\mathrm{miss}}$

CHAPTER 5

SEARCH FOR CHARGED HIGGS BOSONS

5.1 Signature and Event Selection

NEEDS TO BE DONE

5.1.1 Object Definitions

NEEDS TO BE DONE

5.1.2 Event Selections

NEEDS TO BE DONE

5.2 Datasets

NEEDS TO BE DONE

5.2.1 Signal Modeling

NEEDS TO BE DONE

5.3 Background Modeling

NEEDS TO BE DONE

5.4 Analysis Strategy

NEEDS TO BE DONE

5.4.1 Multivariate Analysis Techniques

NEEDS TO BE DONE

5.4.2 Training

NEEDS TO BE DONE

5.4.3 Feature Selection

NEEDS TO BE DONE

5.4.4 Hyperparameter Optimization

NEEDS TO BE DONE

5.5 Systematic Uncertainties

NEEDS TO BE DONE

5.6 Results

CHAPTER 6

CONCLUSION

Appendices

BIBLIOGRAPHY

[1] R. L. Workman et al. "Review of Particle Physics". *PTEP* 2022 (2022), p. 083C01. DOI: `10.1093/ptep/ptac097`.

[2] P. W. Higgs. "Broken Symmetries and the Masses of Gauge Bosons". *Phys. Rev. Lett.* 13 (16 Oct. 1964), pp. 508–509. DOI: `10.1103/PhysRevLett.13.508`. URL: `https://link.aps.org/doi/10.1103/PhysRevLett.13.508`.

[3] F. Englert and R. Brout. "Broken Symmetry and the Mass of Gauge Vector Mesons". *Phys. Rev. Lett.* 13 (9 Aug. 1964), pp. 321–323. DOI: `10.1103/PhysRevLett.13.321`. URL: `https://link.aps.org/doi/10.1103/PhysRevLett.13.321`.

[4] J. Ellis. "Higgs Physics" (Dec. 2013). 52 pages, 45 figures, Lectures presented at the ESHEP 2013 School of High-Energy Physics, to appear as part of the proceedings in a CERN Yellow Report, 117–168. 52 p. DOI: `10.5170/CERN-2015-004.117`. arXiv: `1312.5672`. URL: `https://cds.cern.ch/record/1638469`.

[5] G. A. et al. "Observation of a new particle in the search for the Standard Model Higgs boson with the ATLAS detector at the LHC". *Physics Letters B* 716.1 (2012), pp. 1–29.

[6] G. Branco et al. "Theory and phenomenology of two-Higgs-doublet models". *Physics Reports* 516.1–2 (July 2012), pp. 1–102. ISSN: 0370-1573. DOI: `10.1016/j.physrep.2012.02.002`. URL: `http://dx.doi.org/10.1016/j.physrep.2012.02.002`.

[7] J. R. Andersen et al. "Handbook of LHC Higgs Cross Sections: 3. Higgs Properties" (2013). Ed. by S. Heinemeyer et al. DOI: `10.5170/CERN-2013-004`. arXiv: `1307.1347 [hep-ph]`.

[8] M. Aaboud et al. "Search for charged Higgs bosons decaying via $H^{\pm} \rightarrow \tau^{\pm}\nu_{\tau}$ in the τ+jets and τ+lepton final states with 36 fb^{-1} of pp collision data recorded at $\sqrt{s} = 13$

TeV with the ATLAS experiment". *JHEP* 09 (2018), p. 139. DOI: 10.1007/JHEP09(2018)139. arXiv: 1807.07915 [hep-ex].

[9] CERN. *Facts and figures about the LHC.* URL: https://home.cern/resources/faqs/facts-and-figures-about-lhc.

[10] L. R. Evans and P. Bryant. "LHC Machine". *JINST* 3 (2008). This report is an abridged version of the LHC Design Report (CERN-2004-003), S08001. 164 p. DOI: 10.1088/1748-0221/3/08/S08001. URL: https://cds.cern.ch/record/1129806.

[11] X. C. Vidal and R. C. Manzano. *Lorentz Force Taking a closer look at LHC.* URL: https://www.lhc-closer.es/taking_a_closer_look_at_lhc/0.lorentz_force.

[12] E. Lopienska. "The CERN accelerator complex, layout in 2022. Complexe des accélérateurs du CERN en janvier 2022" (Feb. 2022). General Photo. URL: https://cds.cern.ch/record/2800984.